THE HARDENING OF TYPE 316L STAINLESS STEEL WELDS WITH THERMAL AGING

by

Lauren Juliet Ayers

Submitted to the Department of Nuclear Science and Engineering
in partial fulfillment of the requirements for the degree of

Bachelor of Science in Nuclear Science and Engineering

at the

MASSACHUSETTS INSTITUTE OF TECHNOLOGY

June 2012

Author .....
Department of Nuclear Science and Engineering
May 11, 2012

Certified by .....
Ronald G. Ballinger
Professor, Nuclear Science and Engineering and Materials Science and Engineering
Thesis Supervisor

Certified by .....
Michael P. Short
Research Scientist, Nuclear Science and Engineering
Thesis Reader

Accepted by .....
Dennis Whyte
Chairman, NSE Committee for Undergraduate Students

THE HARDENING OF TYPE 316L STAINLESS STEEL WELDS WITH THERMAL AGING

by

Lauren Juliet Ayers

Submitted to the Department of Nuclear Science and Engineering
on May 11, 2012, in partial fulfillment of the
requirements for the degree of
Bachelor of Science in Nuclear Science and Engineering

Abstract

Welded stainless steel piping is a component of boiling water reactors (BWRs). Reirculation and other large diameter piping are fabricated from Type 304 or 316 stainless steels. Delta ferrite is present in welds, because of its ability to reduce hot cracking; however, its presence can make the microstructure unstable. Delta ferrite is susceptible to spinodal decomposition, a process during which the given material separates into two phases with different compositions and properties, which can lead to brittleness and weakness in the steel. The H.H. Uhlig Corrosion Laboratory is investigating the effect of thermal aging on the physical properties of stainless steel piping. Stainless steel piping, of the same standards of that used in boiling water reactors, was welded and aged at temperatures of 300-400°C for 1,000 - 40,000 hours. The properties of the material were examined using several techniques, including Vickers hardness testing, to evaluate the evolution of hardness of the material, Charpy V-notch testing, to measure the evolution of toughness, and tensile testing. This thesis will focus on the variations in hardness with respect to aging time and location within the weld. Both a low ferrite series (FN=10) and a high ferrite series (FN=13) of Type 316L stainless steel welds were examined for the purposes of this paper. For each series, three materials were tested: an as welded material, a material that was aged at 400°C for 1000 hours, and a material that was aged at 400°C for 5000 hours. A two-dimensional Vickers hardness map was taken of each sample so that how hardness varies within the weld and heat affected zone can be understood. Nanoindentation was also done over small regions of each weld sample, to analyze whether the hardness changes over the dendrite boundaries. The overall hardness of the welds is found to increase to 1000 h and subsequently decrease slightly to 5000 h. The hardness map for each sample was found to be roughly symmetric across the weld centerline, but the hardness values were not found to be consistent along the weld centerline. In general the weld is harder when narrower, and softens as the weld widens. This trend was observed regardless of aging time or ferrite number.

Thesis Supervisor: Ronald G. Ballinger
Title: Professor, Nuclear Science and Engineering and Materials Science and Engineering

Thesis Reader: Michael P. Short
Title: Research Scientist, Nuclear Science and Engineering

Acknowledgments

To Dr. Tim Lucas: I would not be the same student, engineer, or person that I am now had I not come to work for you sophomore year. The lessons you have taught me and the advice you've given me extend far beyond practical lab work, academics, and the professional world. Thank you for many, many invaluable and always enjoyable hours, both in and out of lab. It is because of you that I am proud of my academic achievements here at MIT. (And needless to say, this thesis would not exist without your mentorship).

I would like to thank Professor Ballinger for his support of my undergraduate research in the corrosion lab over the last two and a half years. I am also extremely grateful to Dr. Mike Short, who has helped guide me in the ways of paper-writing, lab work, Lyx, and general making my way towards grad school/the real world in Tim's absence.

On a personal note, many thanks and much love to my parents, Jon and Helaine Ayers, for always taking the time to go the extra mile to support me, and to Marie McGraw, for always being the one to make life bearable in times of stress. Last but most certainly not least, I would like to extend my gratitude to my crew coaches, Claire Martin-Doyle and Amelia Booth, for being an instrumental piece of my personal development over the last few years. Thank you for pushing me to have confidence in myself, for being my constant mentors and inspirations, and for giving me 2+ hours a day of mental sanity and escape from academia. See you next year!

Contents

List of Figures

List of Tables

Chapter 1

Introduction

Stainless steels are used in the piping of boiling water reactors (BWRs) because of their ability to retain their mechanical properties, such as ductility, strength, and toughness, as well as their corrosion resistance at high temperatures [2]. The piping is welded together, with δ-ferrite present in the weld to reduce the susceptibility of hot cracking. However, the δ-ferrite can cause the welds to be unstable at higher temperatures, as it is subject to spinodal decomposition at temperatures as low as 300°C. The decomposition to a brittle, chromium-rich α'-phase and a chromium-depleted α-phase can lead to embrittlement of the weld.

The H.H. Uhlig Corrosion Laboratory has assembled a complete library of aged Type 316L stainless steel welds that simulate the welds present in the piping of BWRs. Stainless steel 316L piping 600 mm in diameter, of the same standards of that used in BWRs, was welded and aged at temperatures of 300, 400, and 430°C for 1,000, 5,000, 10,000, 20,000, and 40,000 hours to create the extensive library of samples. The properties of these welds are being examined through several tests, namely, Vickers hardness testing, to test the macrohardness of the welds, nanoindentation, to test their microhardness, Charpy V-notch testing, to measure the toughness, tensile testing, and fracture toughness. The materials are also being subject to crack growth rate experiments, in a simulated BWR environment.

This thesis concerns hardness mapping done on low ferrite (LF) and high ferrite (HF) material, where low ferrite is defined as a ferrite number (FN) of 10 and high ferrite is defined as a ferrite number of 13. As-welded material, in addition to material aged for 1000 h and 5000 h at 400°C were evaluated for each series. The hardness was mapped over the weld, the heat affected zone (HAZ), and a small portion of the base metal. This extensive mapping allowed the examination of hardness as a function of aging time, position in the weld, and ferrite number. Nanoindentation was performed for each test condition from the high- ferrite series, to examine how the hardness differs between the ferrite and austenite phases.

The overall hardness of the welds is found to increase to 1000 h and subsequently decrease slightly to 5000 h. The hardness map for each sample was found to be roughly symmetric across the weld centerline, but the hardness values were not found to be consistent along the weld centerline. In general the weld is harder when narrower, and softens as the weld widens. This trend was observed regardless of aging time or ferrite number.

Chapter 2

Background

2.1 Spinodal Decomposition

Spinodal decomposition is one process by which an alloy decomposes into equilibrium phases; it occurs when the molar free energy of mixing vs. composition has negative curvature [1], or:

$$\frac{d^2\triangle G}{dX^2} < 0 \tag{2.1}$$

where G is the Gibbs free energy, and X is the composition of the phase. The spinodal is defined at the point in which $\frac{d^2\triangle G}{dX^2} = 0$. Above this point, when the curvature is positive, decomposition happens by nucleation and growth.

During spinodal decomposition, δ-ferrite, an iron-rich phase (known as the α phase) separates to form an additional chromium-rich phase (known as the α' phase) [3] with a sinusoidal composition profile, as illustrated in Figure 2-1. This takes place over two stages. First, a primary wavelength forms, and the difference in concentration between the two phases increases exponentially until the limit as set by the miscibility gap (otherwise known as the two-phase region [1]) is reached. If aging continues, the coarseness/wavelength of each composition increases, but the concentration of each phase will be constant; a simulation of this is shown in Figure 2-2. This results in a sinusoidal composition profile, with a wavelength of approximately five nm or less [4]. This process has been observed in stainless steel welds after several hundred hours of aging at 475°C [5, 6].

While spinodal decomposition is not noticeable in material aged for shorter periods of time at temperatures under 400°C, it does occur once the aging time reaches tens of thousands of hours. In addition to this, the α' phase precipitates grow several orders of magnitude larger than the initial sinusoidal composition profile after extended aging [7]. This phase separation, and the resulting precipitation of the brittle α' phase, causes embrittlement of the weld [7]. As a result, thermal aging of Type 316L stainless steel welds shows an increase in hardness, yield strength, and tensile strength,

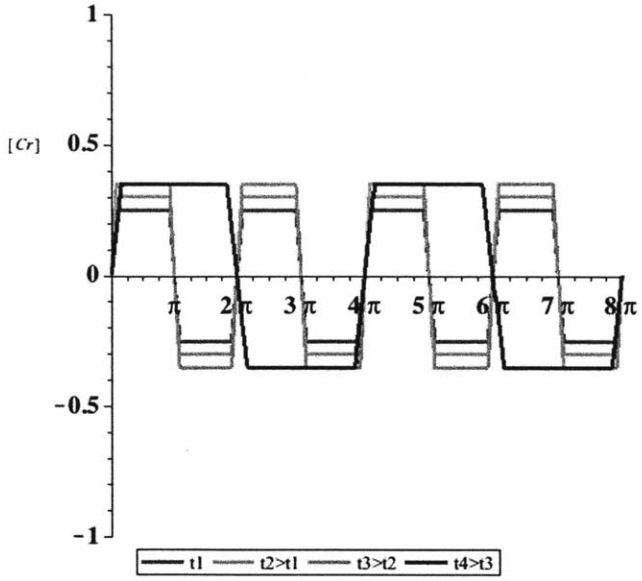

Figure 2-1: The separation of the α and α' phases into a sinusoidal composition profile is shown here, by illustrating the composition profile of one phase; the composition is shown on the y-axis, and the spacial coordinate on the x-axis. After a primary wavelength forms, the difference in concentration between the two phases increases exponentially with time. The length scale eventually coarsens while maintaining fixed phase fractions.

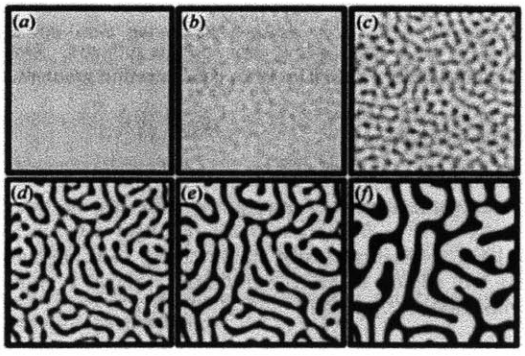

Figure 2-2: A simulation of the decomposition of a system into two distinct phases; figures (a)-(f) show the system as time increases. Initially, the system decomposes into two compositions with a characteristic length scale; as aging continues, the wavelength of each composition increases, while the concentration of each phase is constant. [1]

as well as a decrease in ductility [5]. The embrittlement caused by the precipitation of the α' phase after spinodal decomposition can promote an increase in susceptibility to stress corrosion cracking (SCC), a concern for BWRs as the pipes must last for up to sixty years under a constant tensile stress, which has been measured in some cases to be over 275.8 MPa (40 ksi) [5, 8].

Abe et al. have shown that the solidification mode, or how the weld microstructure is arranged, may affect the kinetics of spinodal decomposition [9]. The solidification mode is affected by the degree of constitutional supercooling [10]. After thermal aging for 500, 1000, 2000, 4000, and 8000 hours was performed at 335°C on two types of 316L stainless steel weld metals with different solidification modes, differences in the morphology of the microstructure and the hardening behaviors were examined. The ferrite phase hardness increased, while the austenite phase hardness stayed roughly the same [9]. These results suggest that spinodal decomposition occurs only in the δ-ferrite phase. As the hardening rate of the ferrite was faster for the primary austenite solidification mode than the primary ferrite solidification mode, it is believed that the solidification mode affects the kinetics of spinodal decomposition.

2.2 Stress Corrosion Cracking (SCC)

Ultimately, spinodal decomposition can lead to stress corrosion cracking (SCC), a phenomenon that only occurs in an alloy when three conditions are present: the alloy must be a susceptible alloy in a corrosive environment and subject to a tensile stress. The presence of these three conditions can result in the unexpected failure of the material [11].

Type 316L stainless steel in BWRs match this criteria. Residual welding stress contributes to the tensile stress; stresses greater than 275.8 MPa (40 ksi) have been recorded in the HAZ of stainless steel piping [8]. The BWR environment is high purity water containing residual dissolved oxygen, hydrogen peroxyde, and hydrogen from radiolysis or addition (Hydrogen), creating a susceptible environment [8]. Many alloys, including Type 316L stainless steel, are susceptible to SCC, despite being corrosion resistant in most other environments [12].

2.3 Vickers Hardness

The process commonly used to measure hardness is the Vickers hardness test, developed in 1925 [13]. A square-based pyramidal diamond indenter is pushed into the surface of the specimen with a predetermined force. After the indenter is removed, the diagonals of the resulting impression are measured, and the hardness number, noted as HV for Vickers testing, is calculated by the following equation:

$$HV = 2P\frac{sin(\frac{\alpha}{2})}{d^2} = 1.8544\frac{P}{d^2} \tag{2.2}$$

where P is the force in kilogram-force, d is the mean diagonal of the impression in millimeters, and α is the face angle of the pyramidal diamond indenter, 136° in this case [14]. To measure the hardness of a weld before and after aging, 2D hardness maps of representative welds are developed. Vickers hardness testing was performed incrementally over the entire weld and Heat Affected Zone (HAZ) region, with a minimum test point separation distance of three times the diagonal measurement of the indent, and the results are typically plotted graphically [15]. This allows changes over the whole surface of the weld to be examined, without the data points interfering with each other due to work hardening and plastic deformation.

2.4 Ferrite Number

The ferrite number (FN) is a measure of the ferrite content of the weld. The FN is determined using magnetic methods (as the ferrite phase is magnetic) and is roughly approximate to the percentage of ferrite in the weld. The FN can be found from the DeLong diagram, shown in Figure 2-3 [16]. To use the diagram, a weld metal analysis is performed and the nickel and chromium equivalents are calculated.

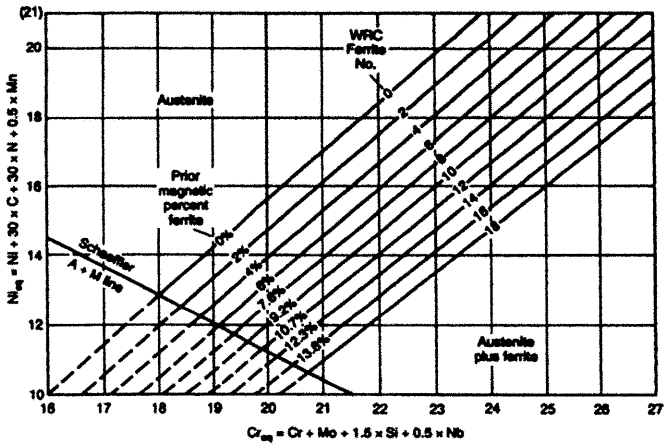

Figure 2-3: DeLong constitutional diagram for stainless steel welds. From [16]

2.5 Nanoindentation

Nanoindentation is the process of applying an indentation hardness test, such as the Vickers hardness test discussed in Section 2.3, on a nanoscale. The problems involved with scaling down such a process include locating and measuring the contact area, as it is very small. Instead, the indenter geometry,

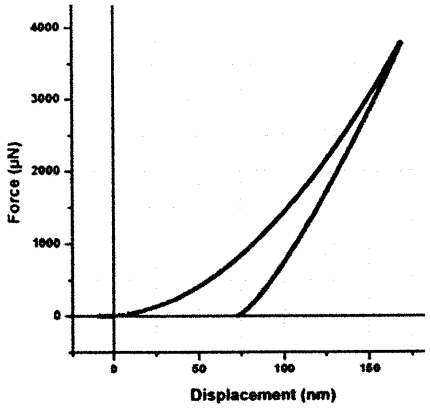

Figure 2-4: An example of a load displacement curve, which can be used to determine mechanical properties of the material. [13]

usually a three-sided pyramid (known as a Berkovich tip), is known to high precision; during the indentation, the load and the depth of penetration is continuously recorded, producing a load-displacement curve (an example of this is shown in Figure 2-4). This information can be used to determine mechanical properties of the material [17].

2.6 Summary of Relevant Previous Results

This project is an extension of the doctoral projects of Dr. Timothy Lucas [12]. His research was focused on the effects of thermal aging and the BWR environment on properties of Type 316L stainless steel welds. Testing was performed on the extensive library of aged and unaged welds assembled by the H.H. Uhlig Corrosion Laboratory. Samples of welded piping of the exact standards of BWRs, with ferrite numbers of 10 and 13, were obtained and cut into blanks. These samples were aged at temperatures of 430°C and 400°C for 1,000, 5,000, and 10,000 hours, and at 350°C and 300°C for 5,000, 20,000, and 40,000 hours. The specimens were then subject to Charpy V-notch testing and fracture toughness tests, both at room temperature and at 288°C. For comparison, these tests were also performed on as-welded samples. While this thesis examines the changes in hardness of the steel as a result of thermal aging, the changes in tensile strength and fracture toughness are also relevant. For FN=10 and FN=13, material aged for 1,000 h and 5,000 h at 400°C were tested. The aged samples showed small changes when tested at room temperature. For the low-ferrite 5000h aged sample, there was an increase in yield strength, from 480 MPa as-welded to 496 MPa aged, an increase in tensile strength, from 645 MPa as-welded to 670 MPa aged, and a decrease in ductility, from 44% RA (reduction in area) as-welded to 39% RA aged.

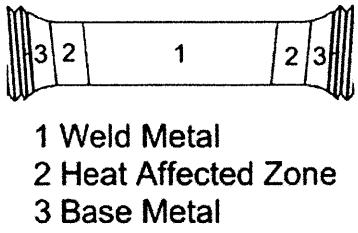

Figure 2-5: Tensile specimen orientation within the weld sample. [12]

2.6.1 Tensile Testing

Tensile testing was performed at 25°C on all as-welded and aged samples, and at 288°C for as-welded samples that had been aged at 400°C for 1,000, 5,000, and 10,000 hours. Testing was carried out in accordance with the ASTM E8 standard on an Instron® 8500R load frame [18]. Figure 2-5 shows the orientation of the tensile specimen relative to the weld zones.

A selection of the results are reported in Figure 2-6, adapted from [12]. Hardness testing for this work was performed at room temperature on as-welded samples and samples that had been aged for 1000 and 5000 hours at 400°C, for high and low ferrite welds. Only results from tensile samples tested at 25°C are shown here, such that they are comparable to the hardness data collected in this thesis.

2.6.2 Fracture Toughness Testing

The 1T-CT (one inch (2.54 cm) thick, compact tension) fracture toughness specimens were constructed and the fracture toughness tests were carried out in accordance with the ASTM E1820 standard [19]. Both atmospheric and in-situ testing were performed. For samples tested in air, the load was applied by an Instron® 8500R load frame, with temperature control provided by a 6.9 kW Thermocraft furnace [12].

A selection of the results are reported in Figure 2-8, adapted from [12]. As in Section 2.6.1, only results from fracture toughness samples tested at 25°C in air have been shown here, such that they are comparable to the hardness data.

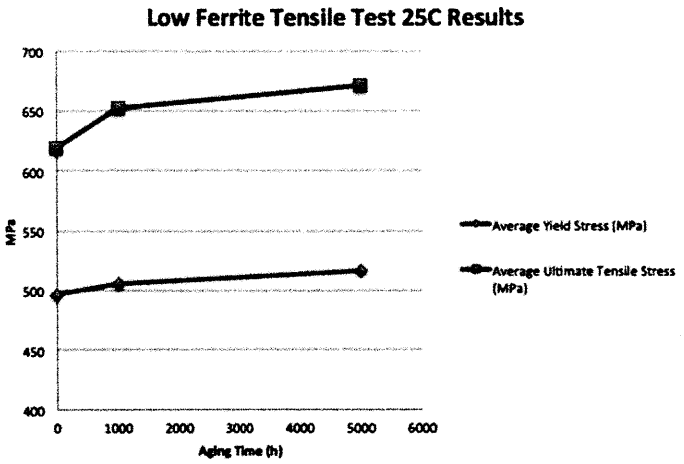

(a) Average yield stress and ultimate tensile stress for low ferrite samples at various aging times aged at 400°C. Adapted from [12]

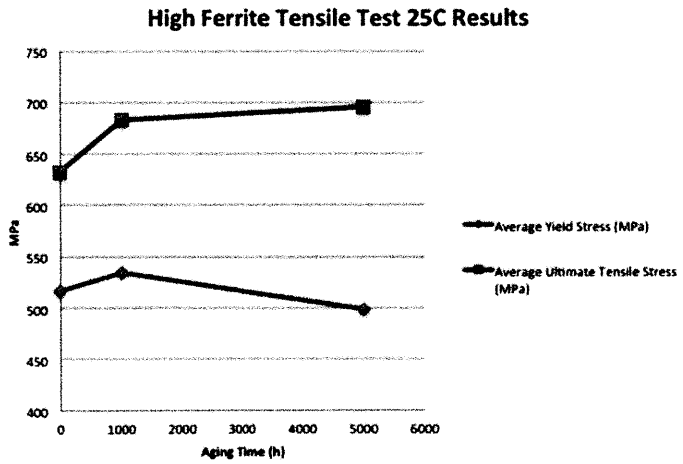

(b) Average yield stress and ultimate tensile stress for high ferrite samples at various aging times aged at 400°C. Adapted from [12]

Figure 2-6: Results from tensile tests performed at room temperature on as-welded samples and various samples aged at 400°C, for low and high ferrite welds. Adapted from [12]

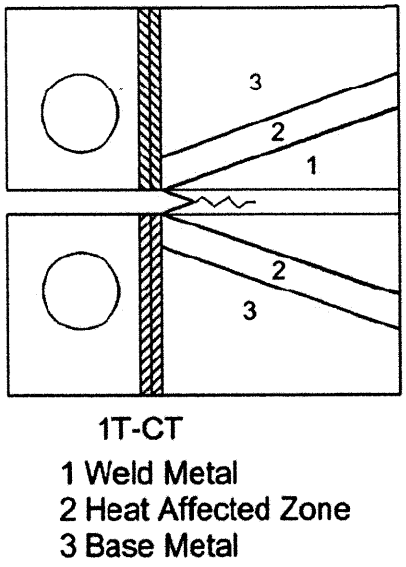

Figure 2-7: The orientation of the 1T-CT fracture toughness specimen within the sample. [12]

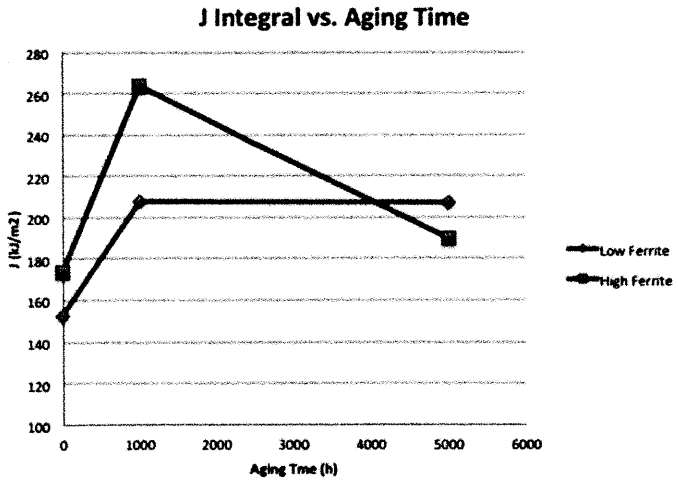

Figure 2-8: Results from fracture toughness tests performed at 25°C in air. [12]

Chapter 3

Experimental Procedures

This thesis explores the 2D Vickers hardness behavior of a series of low- and high-ferrite welds. Each series contains an as-welded sample, in addition to samples aged for 1000 h and 5000 h, all at 400°C.

3.1 The Weld Samples

The materials tested were manufactured in the same manner as those used in BWRs. To obtain the samples, Type 316L stainless steel piping, 600mm in diameter, was joined using two heats of Type 316L filler metals by gas tungsten arc welding (GTAW), the same process used in the construction of large BWR piping.

3.1.1 Type 316L Stainless Steel

Type 316L stainless steel is an iron-chromium-nickel-molybdenum alloy. Two compositions of Type 316L stainless steel weld wire were obtained for this project. The compositions are given in Table 3.1 . The "L" stands for low carbon, which, along with the addition of molybdenum, increases the corrosion resistance of the alloy. This is one reason for its prevalence in BWRs. Other alloying elements commonly present in Type 316L stainless steel include manganese, silicon, sulfur, and copper [12].

Chromium increases the corrosion resistance of the alloy. However, it can also participate in the formation of an embrittling phase when the steel undergoes spinodal decomposition. Nickel, meanwhile, promotes the austenite phase. Molybdenum stabilizes the ferrite, and increases the

Specification	Fe	C	Mn	Si	S	P	Cr	Ni	Mo	Cu
316L-WO21437	Bal.	0.022	1.85	0.44	0.001	0.21	19.34	12.68	2.51	0.26
316L-HT94789	Bal.	0.15	1.75	0.35	0.14	0.14	19.2	12.3	2.61	0.05

Table 3.1: Composition of type 316L stainless steel weld wires [12]

strength of the alloy at high temperatures. Manganese combines with sulfur, which is added to increase machinability of the steel but can lead to hot cracking in the alloy if it combines with iron. Silicon does not aid in the formation of ferrite or austenite; however, it decreases viscosity of the weld pool and scavenges oxygen. [12]

3.1.2 Gas Tungsten Arc Welding (GTAW)

GTAW was chosen because of its low contamination rate, and because the ease of the process allows for automated welding [12]. GTAW employs an inert shielding gas in order to keep the weld and the tungsten electrode both shielded from the atmosphere and oxygen free [20]. This prevents impurities from the atmosphere from contaminating the weld. Contaminates are present in the weld, however, as the parent metals themselves contain impurities. The melting of the tungsten electrode can also introduce impurities into the weld.

3.1.3 Weld Sample Sectioning

The welded sections were cut axially out of the pipe, as shown in Figure 3-1a. The welded rings were then sectioned radially, as shown in Figure 3-1b. The samples were configured such that hardness testing over one plane could cover the weld metal, the HAZ, and the base metal.

3.2 Sample Preparation

Samples were cut from the blank metal using wire electro-discharge machining (EDM). The surface of each weld was then polished to a mirror finish using a Buehler Automet-3 polisher. Each sample was ground with 300, 600, 800, and 1200 grit silicon carbide papers before being polished with a 0.05 μm alumina slurry, in accordance to the standards set by ASTM standard E92-82 [21]. After polishing was completed, the samples were etched using Murakami's reagent, made by dissolving 10 g of potassium hydroxide in 50 mL of water heated to 80°C. 10 g of potassium ferricynide (KCN) was added, and the reagent was stirred until the KCN dissolved. The surface of each polished weld sample was immersed for 30 second intervals, until the weld was visible on the polished surface. Figure 3-2 shows the polished, etched weld.

3.3 Vickers Hardness Mapping

Hardness testing was perfomed in accordance with ASTM standard E92-82 [21] on a LECO Model LM 247AT micro-hardness tester with a Vickers indenter. This machine can be seen in Figure

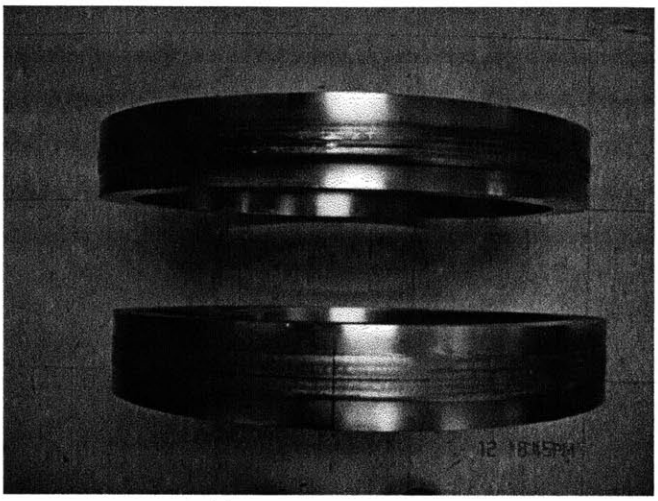

(a) Two typical weld rings

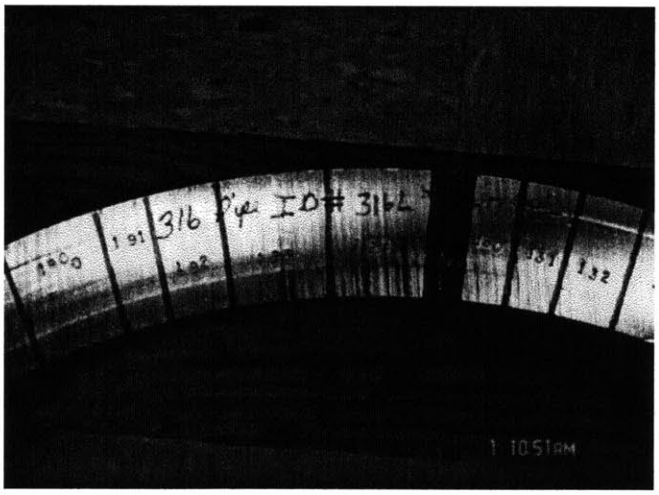

(b) A sample sectioning diagram from a weld ring

Figure 3-1: Weld sample configuration within pipe

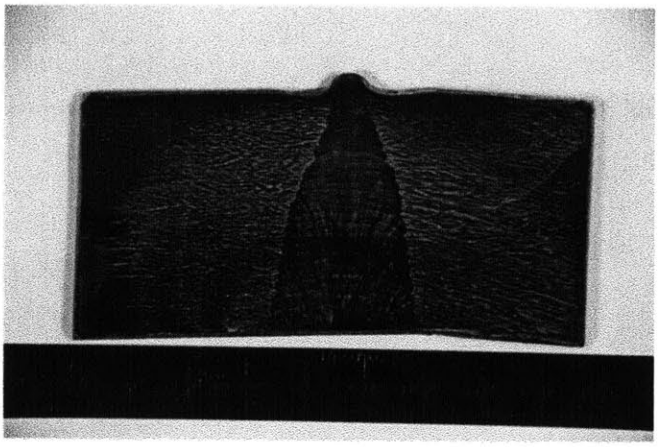

Figure 3-2: A weld section, polished to 0.05 μm and etched with Murakami's reagent.

3-3. The machine was calibrated using a hardness standard of 543 HV. The samples were placed under the lens of the LECO machine, with an image of the surface magnified 500x displayed on the computer connected to the machine. After the region of interest was in focus, the test was run; the lens automatically rotated out and the diamond indenter rotated into position. The ConfiDent and PAXCAM software packages were used to determine the depth of each indent and the hardness of each point.

The Vickers hardness tests were performed with a test load of 500 gf and a dwell time of 15 seconds. Once the test was completed, the lens rotated back into position, allowing the size of the indent to be measured. Once the corners were manually identified, the computer used the lengths of the diagonals, along with equation 2.2, to calculate the Vickers hardness number for that point. A picture of an indentation can be seen in Figure 3-4. This data point was taken within the HAZ of the 1000 h aged low-ferrite sample; the diagonals were measured to be 65.66 μm (horizontal) and 65.48 μm (vertical), giving an HV of 216. The pink and blue lines identify the lengths of the horizontal and vertical diagonals, respectively.

The hardness was evaluated in a grid over the surface of the sample, with indents performed 1.905 mm (3/40 of an inch) apart. This distance was chosen in order to prevent effects from work hardening. Measurements were taken in a line across the weld, until those obtained were consistently measured to be near 170HV. This value was chosen to demarcate the end of the HAZ and the start of the base metal. For the first sample tested, the low-ferrite 1000 h-aged sample, many points within the base metal were taken to ensure consistency of hardness values outside of the HAZ. The measurements were recorded and plotted in Excel. The region mapped for each sample is shown in Figure 3-5.

Figure 3-3: The LECO Model LM 247AT Hardness Tester with a Vickers indenter used in this study.

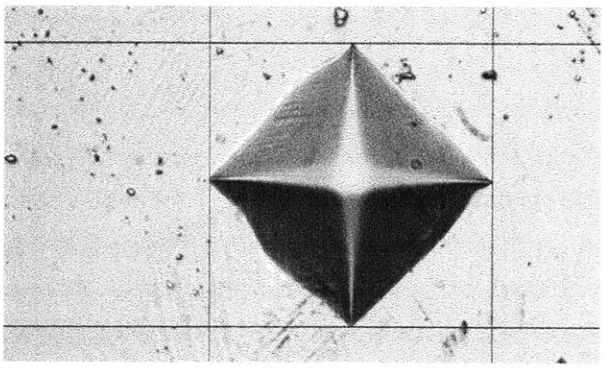

Figure 3-4: An indentation (magnified 500x) left by the diamond tip in the HAZ. The diagonals measure 65.66 μm (horizontal) and 65.48 μm (vertical).

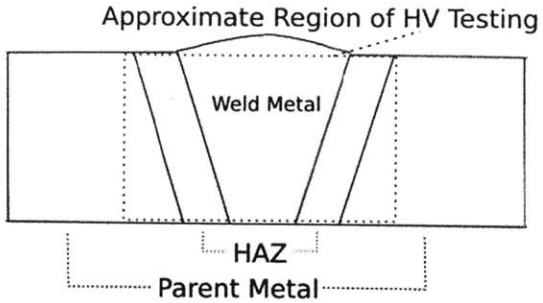

Figure 3-5: The region of the weld face covered by Vickers Hardness testing. The entire weld and HAZ region is tested.

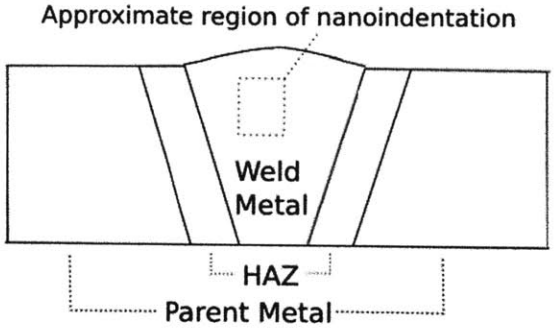

Figure 3-6: The approximate region cut from the welds to perform nanoindentation

3.4 Nanoindentation

Microhardness testing is carried out on too large a scale to distinguish between the ferrite and austenite regions, as the Vickers indents are on the order of 60 μm across, while the dendrites are roughly 10 μm wide. Thus, nanoindentation was performed on an as-welded, high ferrite (HF) sample, in addition to HF samples aged for 1000 h and 5000 h, so that the points could be taken on the same length scale as relevant microstructural features. The nanoindentation samples were prepared in a similar way to the Vickers hardness samples, except that a much smaller sample was cut. To keep as many variables as possible consistent across the three samples, a section from the same region of each sample was cut and prepared, shown in Figure 3-6. After each small section was cut from a material, it was polished to 0.05 μm in the same manner as the Vickers hardness samples (see section 3.2), and etched with Murakami's reagent.

Nanoindentation was performed using a Hysitron TriboIndenter. Ten points were taken per sample, five within the dendrites and five between the dentrites, in order to examine the differing properties of different microstructural regions. A camera was used to manually determine an optimal position to take each test point, to ensure that each point was either fully within or outside of a dendrite. The maximum load was approximately 1 mN (approximately 0.1 gf), with a load time of

12.1 s. The nanohardness was recorded in GPa, which was then converted to HV for comparason to the hardness mapping.

Chapter 4

Results

4.1 Hardness Mapping

The overall weld hardness can be seen to increase after aging for 1000 h, and then decrease slightly after 5000 h. Maps of the hardness results for the HF and LF materials can be seen in the figures below. Figures 4-1a, 4-1b, and 4-1c show the HF materials, for the as-welded, 1000 h, and 5000 h conditions respectively, and figures 4-2a, 4-2b, and 4-2c show the LF results, for the as-welded, 1000 h, and 5000 h conditions respectively. Figures 4-3a and 4-3b show the average hardness values for the weld and the HAZ for the LF and HF materials, respectively. A summary of the results can be found in Table 4.1. The average hardness of both the weld and HAZ, for both the HF and LF materials, increases after aging for 1000 h and then decreases after 5000 h. This same trend has been observed in the testing of fracture toughness specimens, while in general tensile specimens show a jump in yield stress and ultimate tensile stress after aging for 1000 h and then a lesser increase after 5000 h.

While the average hardness increased and then decreased for both series tested in this work, the minimum hardness found within the weld region stayed roughly the same. Figures 4-4a and 4-4b show the maximum and minimum hardness values found within the weld region for the HF and LF series, respectively.

Aging Time (h)	Weld Avg (HV)	HAZ Avg (HV)	Weld Max (HV)	Weld Min (HV)
0 (LF)	236	231	283	191
1000 (LF)	245	242	264	231
5000 (LF)	241	216	284	200
0 (HF)	246	233	282	205
1000 (HF)	267	236	302	238
5000 (HF)	260	233	298	207

Table 4.1: Summary of average and maximum and minimum hardness values.

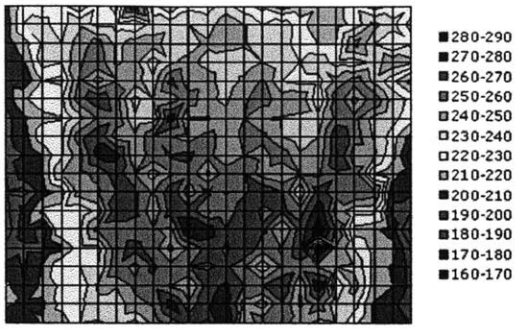

(a) Vickers Hardness map for the HF as-welded sample.

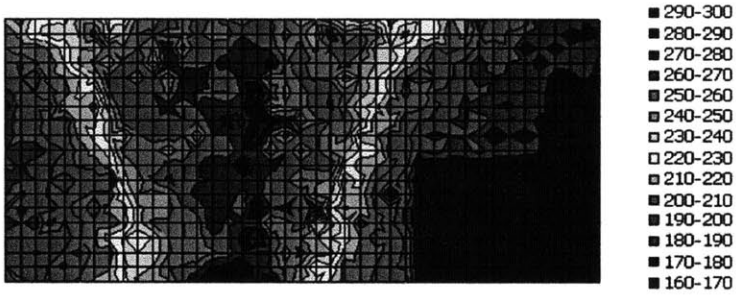

(b) Vickers Hardness map for a HF sample aged at 400̊ C for 1000 hours.

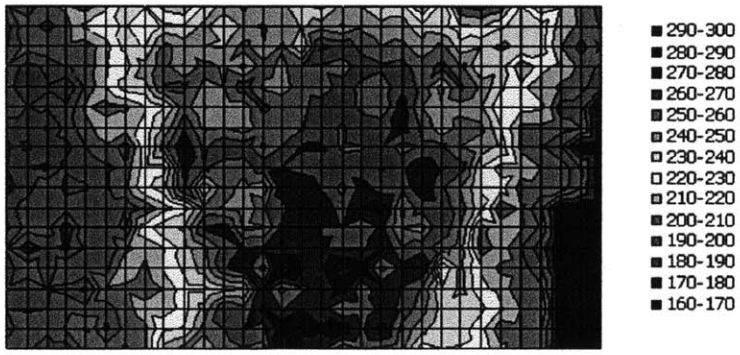

(c) Vickers Hardness map for a HF sample aged at 400̊ C for 5000 hours.

Figure 4-1: Hardness maps for the high ferrite (FN=13) 316L stainless steel welds.

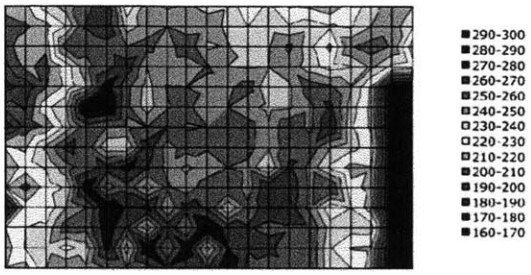

(a) Vickers Hardness map for the LF as-welded sample.

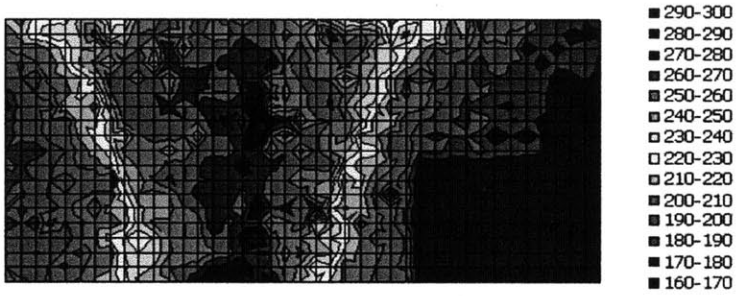

(b) Vickers Hardness map for a LF sample aged at 400̊ C for 1000 hours.

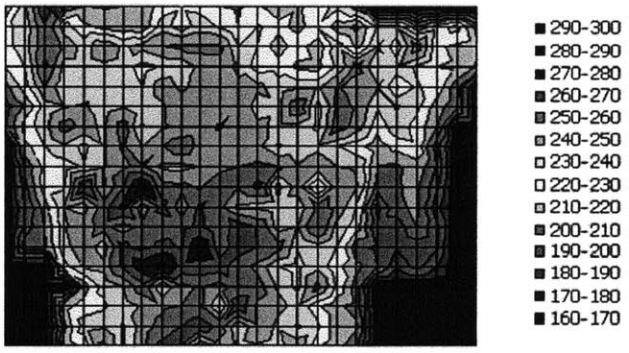

(c) Vickers Hardness map for a LF sample aged at 400̊ C for 5000 hours.

Figure 4-2: Hardness maps for the low ferrite (FN=10) series of 316L stainless steel welds.

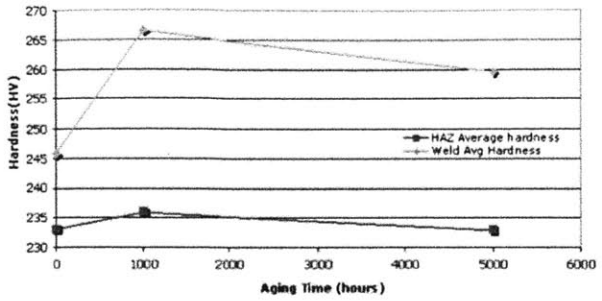

(a) Weld and HAZ average hardness for the high ferrite series.

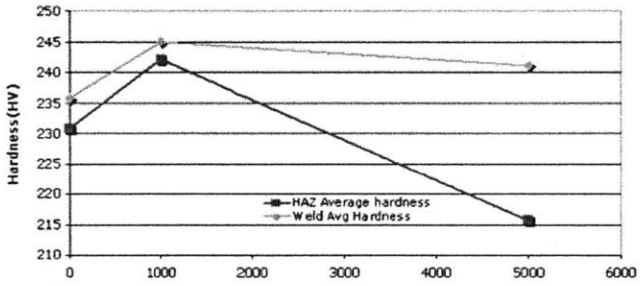

(b) Weld and HAZ average hardness for the low ferrite series.

Figure 4-3: Average hardness vs. aging time for the weld region and HAZ of the high (a) and low (b) ferrite series.

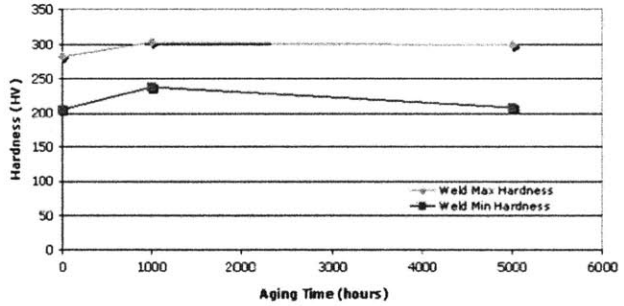

(a) Weld minimum and maximum hardness for the HF (FN=13) series.

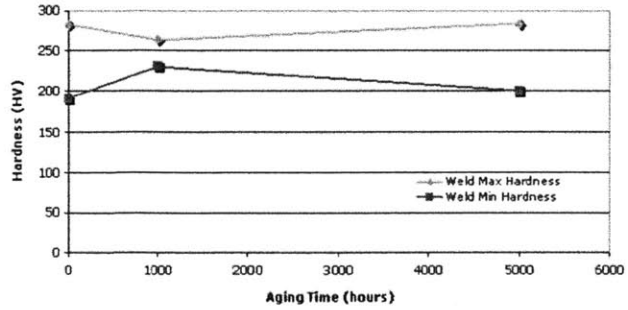

(b) Weld minimum and maximum hardness for the LF (FN=10) series.

Figure 4-4: The minimum and maximum hardness found within the weld region for each of the six samples, with respect to aging time and ferrite number.

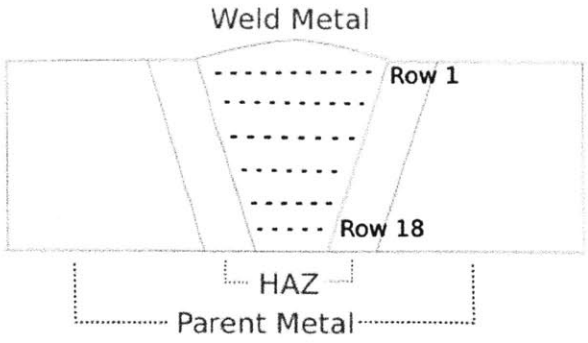

Figure 4-5: Schematic of how row averages were taken. All the points in a row were averaged so that the average hardness could be plotted with respect to position within the weld "V".

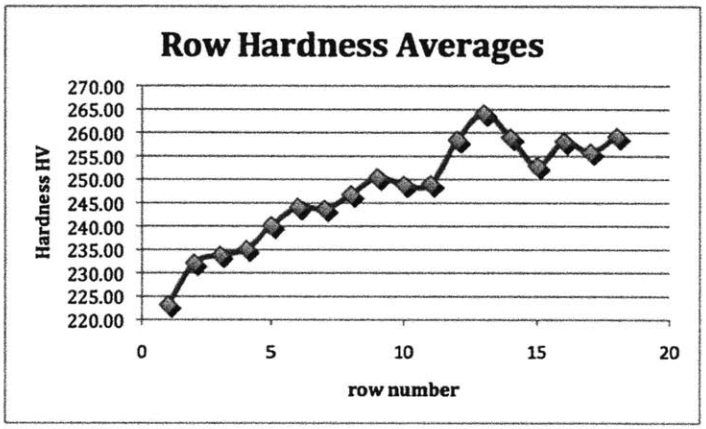

Figure 4-6: Average hardness vs. row number, with row 1 at the top (widest) part of the weld, and row 18 at the bottom (narrowest) point of the weld. The row scheme is shown graphically in Figure 4.5.

The results are observed to be approximately symmetric across the weld centerline, but not symmetric perpendicular to the weld centerline. The weld is hardest when it is narrowest, at the innermost radius of the pipe. For each of the samples, the weld hardens as it narrows. This trend is observed in all six hardness maps. An average of all the points in each row was taken the HF as-welded sample. The shape of the weld region forms a "V", symmetrical over the weld centerline. The rows of indentations run perpendicular to the weld centerline, giving an average hardness as a function of the width of the weld "V"; the rows are shown in Figure4-5. The results of average hardness values versus row number are shown in Figure ??. These results indicate that the weld hardness is not symmetric across the weld centerline.

4.2 Nanoindentation Results

The average results for nanoindentation are plotted in Figure 4-7. The average hardness in the matrix is found to be highest in the as-welded sample, and decreases to 1000h; however, the average hardness is roughly constant at 1000h and 5000h. The average hardness in the dendritic region, meanwhile, is found to increase after aging for 1000 h, and then decreases after 5000 h, as seen in the hardness map of the entire weld region shown in Figure 4-3. However, unlike the macrohardness results, the hardness of the dendritic region decreases below the as-welded value after aging for 5000 h.

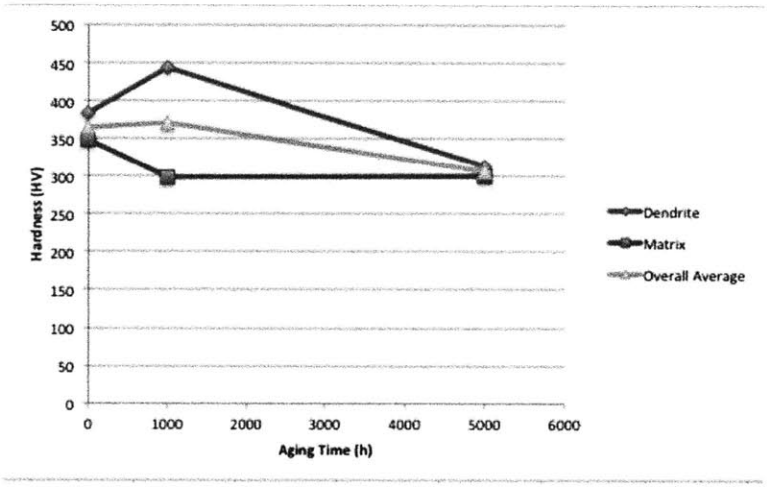

Figure 4-7: The average of the points taken in the dendrite region, the matrix, and the overall average for each sample in the HF series.

The constant hardness in the matrix region in the aged samples indicates that further testing should be done, to determine whether the decrease in hardness in the matrix region from the as-welded sample to the aged samples is accurate, as the literature supports the idea that the hardness in the matrix region may stay approximately constant with aging [9].

Chapter 5

Discussion

5.1 Vickers Hardness

While the 2D hardness mapping procedure is a new approach, M. Shafty performed a linear analysis across Type 316L stainless steel welds of different aging times between 100 h-5000 h at 400 ° C [22]. The report found that the weld metal had a 40% higher hardness value than the base metal [22]. This agrees with the LF 1000 h sample, for which many base metal points were taken. The increase in hardness between the base metal (173 HV) and the weld (245 HV) was about 42%. Shafty reports that the hardness increases following up to 500 h of aging, but decreases after 1000 h and continues to decrease through 5000 h. This is consistent with the hardness data found in this study. There is a large increase in average hardness between the as-welded and the material aged for 1000 h, but the average hardness decreases between 1000 h and 5000 h aging time. The suggested explanation for the increase to 500 h, decrease to 1000 h, increase to 2000 h and decrease for aging beyond this found by Shafty is a balance between recovery processes and precipitation [22]. It is suggested that the decrease after 500 h aging is due to recovery processes, and that aging beyond this time will result in precipitation, increasing the hardness [22]. Upon aging past 2000 h, a balance occurs between recovery processes, which involve the formation and growth of subgrain boundaries [23] and precipitation [22].

The minimum hardness found within the weld region for this thesis remained roughly the same for both the LF and HF materials; a possible reason for this may be that spinodal decomposition occurs only in the ferrite phase. A study by Abe et al. tested the Vickers hardness of the ferrite and austenite phases in 316L welds aged from 500-10,000 h at 335°C [24]. The report showed that while the austenite phase stayed at approximately the same hardness as the aging time increased, the ferrite phase increased in hardness from about 210 HV before aging to over 300 HV after 10,000 h, following a roughly logarithmic trend. These hardness values were found by averaging five points

with the ferrite phase and austenite phase; they were not the results of a 1D survey or a 2D map.

5.2 2D Hardness Mapping

The results from this thesis show that in order to examine the overall hardness of a weld 0D and 1D hardness surveys are not sufficient. A 2D map is necessary because hardness varies in two dimensions. In addition to increasing from the base metal through the HAZ and weld, the hardness varies in the direction parallel to the fusion line. As the weld becomes wider, it softens, with the hardest points at the narrowest part of the V. One possible reason for this is that the narrower sections of the weld cool more quickly as they are closer to the colder parent metal. Averaging a few measurements within the weld or performing a 1D test ignores this variation and does not give complete information about the hardness of the weld. This can lead to inaccurate trends if different parts of the different samples are measured and compared.

5.3 Nanoindentation

It is commonly suggested that dendritic spacing has an effect on hardness; the closer the dendrites are spaced together, the harder the material [24]. This is true of the high-ferrite materials tested, which were consistently harder than the low-ferrite materials. It has also been suggested that the dendrite morphology is an important factor in determining the hardness [12]. Some dendrites are at different angles to the Vickers tip, which leads to different planes of exposure. The directional dependence on tensile properties of crystals may also be reflected in the dendrite morphology [25], leading to variations in hardness depending on the orientation of the dendrites.

In another study by Abe et al, samples expressing the primary ferrite solidification mode and the primary austenite solidification mode for 316L stainless steel welds were hardness tested [9]. The points were taken on a scale such that the points were either completely within the austenite or within the ferrite region. It was suggested that the solidification mode can affect the kinetics of spinodal decomposition. The age hardening rate of the δ-ferrite was faster for the primary austenite solidification mode than the primary ferrite solidification mode. However, for samples of both modes, the austenite region stayed roughly consistent with aging time, while the ferrite mode hardened as aging time increased [9]. This is a possible explanation for why the materials discussed in this thesis have a roughly consistent minimum weld hardness, regardless of aging time.

Chapter 6

Conclusions and Future Work

2D Vickers hardness maps of both low ferrite (FN=10) and high ferrite (FN=13) welds were examined in the context of BWR coolant pipe weld integrity. As-welded material was tested for each series, in addition to materials aged at 400°C for 1000 h and 5000 h. Nanoindentation was also performed to examine the hardness of the ferrite and austenite phases. The conclusions can be summarized as follows:

1. Average weld hardness increases after aging for 1000 h, and subsequently decreases after 5000 h for both high ferrite and low ferrite welds.
2. The hardness map is roughly symmetric across the weld centerline.
3. Hardness values are not consistent along the weld centerline; the weld is in general harder when narrower, and softens as the weld widens. This trend was observed regardless of aging time or ferrite number, showing that the hardness is dependant not only on the weld, but also on the location of hardness testing within the weld.
4. The minimum hardness within the weld does not change significantly with aging time.
5. Nanoindentation shows the average hardness across the austenite region to be consistent, with the exception of the as-welded material, while the δ-ferrite region increases in hardness after aging for 1000 h and then decreases after 5000 h.

Future work should examine the difference in hardness trends between the ferrite region and the austenite region in more detail using nanoindentation. The hardness of the austenite region was found to be consistent for the 1000 h- and 5000 h-aged samples; nanoindentation should be repeated on further aged samples, in order to determine if this consistency is a trend.

Bibliography

[1] R.W. Balluffi, S.M. Allen, W.C. Carter, and R.A. Kemper. *Kinetics of Materials.* John Wiley & Sons, Inc, 2005.

[2] William D. Callister. *Materials Science and Engineering, an Introduction.* John Wiley & Sons, Inc., 2000.

[3] J. Hillard. *Phase Transformations, Spinodal Decomposition.* ASM International, 1970.

[4] M.K. Miller et al. Spinodal Decomposition in Fe-Cr Alloys: Experimental Study at the Atomic Level and Comparison with Computer Models - I. Introduction and Methodology. *Acta Metallurgica*, 43:3385–3401, 1995.

[5] J.H. Kim and R.G. Ballinger. Stress Corrosion Cracking Crack Growth Behavior of Type 316L Stainless Steel Weld Metals in Boiling Water Reactor Environments. *Corrosion*, 64:645, 2008.

[6] J.B. Vogt, K. Massol, and J. Foct. Role of the Microstructure on Fatigue Properties of 475C Aged Duplex Stainless Steels. *International Journal of Fatigue*, 24:627–633, 2002.

[7] H.M. Chung and O.K. Chopra. Kinetics and Mechanism of Thermal Aging Embrittlement of Duplex Stainless Steels. In *Materials and Components Technology Division, Argonne National Laboratory*, 1987.

[8] Michael Fox. An Overview of Intergranular Stress Corrosion Cracking in BWRs. *J. Materials for Energy Systems*, 1:3–13, 1979.

[9] H. Abe and Y. Watanabe. Low-temperature aging characteristics of type 316L stainless steel welds: Dependences on solidification mode. *Metallurgical and Materials Transactions*, 6, 2008.

[10] Sindo Kou. *Welding Metallurgy, Second Edition.* Wiley-Interscience, Jon Wiley & Sons, 2003.

[11] G.S. Was. *Fundamentals of Radiation Materials Science.* Springer Berlin Heidelberg, New York, 2007.

[12] T.R. Lucas. *The Effect of Thermal Aging and Boiling Water Reactor Environment on Type 316L Stainless Steel Welds.* PhD thesis, Massachusetts Institute of Technology, 2011.

[13] Vickers Test, February 2012. URL http://www.instron.us/wa/applications/test_types/hardness/vickers.aspx.

[14] ASTM, Standard Test Method for Knoop and Vickers Hardness of Materials (E384-11), ASTM International, 2012, .

[15] V. Shankar G. Srinivasan, A.K. Bhaduri and S.K. Ray. Impact Toughness of 316 Stainless Steel Weld Metal on Elevated Temperatures Aging. *Science and Technology of Welding and Joining*, 12, 2007.

[16] *Weld Integrity and Performance.* ASM International, 1997.

[17] G.M. Pharr W.C. Oliver. Measurement of Hardness and Elastic Modulus by Instrumented Indentation: Advances in Understanding and Refinements to Methodology. *J. Mater. Res.*, 19: 3–20, 2003.

[18] ASTM International, Standard Test Models for Tension Testing of Metallic Materials (ASTM E8-04), ASTM International, 2004, .

[19] ASTM, Standard Method for Measurement of Fracture Toughness (E1820-01), ASTM International, 2001, .

[20] Miller Welds TIG Handbook, Chapter I - The GTAW (TIG) Process, http://www.millerwelds.com/resources/TIGhandbook/ .

[21] ASTM, Standard Test Method for Vickers Hardness of Metallic Materials, e92-82, ASTM International, 2003.

[22] M. Shafty. Embrittlement Prediction of Aged Austenitic Stainless Steel Welded Components using Hardness Measurements. *Egyptian Journal of Solids*, 28, 2005.

[23] E. Letofsky and H. Cerjak. Metallography of 9-12Cr steel power plant weld microstructures. *Institute for Materials Science, Welding and Forming, University of Technology, Koperniksug*, 2002.

[24] H. Abe, K. Shimizu, and Y. Watanabe. Low-Temperature Aging of Delta Ferrite in 316L SS Welds; Changes in Mechanical Properties and Etching Properties. *Journal of Power and Energy Systems*, 2, 2008.

[25] R. Hertzberg. *Deformation and Fracture Mechanics of Engineering Materials.* John Wiley & Sons, Inc, 1996.